Hydrogen-Evolution Reaction

Deutsche Ausgabe: DOI: 10.1002/ange.201600686
Internationale Ausgabe: DOI: 10.1002/anie.201600686

Ultrasmall Cu_7S_4@MoS_2 Hetero-Nanoframes with Abundant Active Edge Sites for Ultrahigh-Performance Hydrogen Evolution

Jun Xu[+], Jiabin Cui[+], Chong Guo, Zipeng Zhao, Rui Jiang, Suying Xu, Zhongbin Zhuang, Yu Huang, Leyu Wang, and Yadong Li*

Abstract: *Increasing the active edge sites of molybdenum disulfide (MoS_2) is an efficient strategy to improve the overall activity of MoS_2 for the hydrogen-evolution reaction (HER). Herein, we report a strategy to synthesize the ultrasmall donut-shaped Cu_7S_4@MoS_2 hetero-nanoframes with abundant active MoS_2 edge sites as alternatives to platinum (Pt) as efficient HER electrocatalysts. These nanoframes demonstrate an ultrahigh activity with 200 mA cm^{-2} current density at only 206 mV overpotential using a carbon-rod counter electrode. The finding may provide guidelines for the design and synthesis of efficient and non-precious chalcogenide nanoframe catalysts.*

The hydrogen-evolution reaction (HER), as a fundamental step of electrochemical water splitting, always requires an efficient and cost-effective catalyst to achieve fast kinetics for practical applications.[1] Platinum (Pt) has been identified as the most active HER catalyst, whereas its low abundance and high cost hinder the large-scale application.[2] Nanostructured molybdenum disulfide (MoS_2) has been widely investigated as a promising and inexpensive alternative to platinum for HER.[3] Both experimental[4] and computational[5] studies have suggested that the catalytic activity of MoS_2 is localized to rare edge sites of the layered structure.[6] That is, the unsaturated sulfur atoms on the edges play a crucial role in HER catalysis.[4] To this end, various strategies have been employed to engineer nanostructured MoS_2 to improve the number of exposed edge sites for enhanced HER activity.[4] For example, chemical exfoliation,[7] growing MoS_2 on various supports,[8] and template methods[9] have been devoted to the fabrication of few/mono-layer MoS_2 nanostructures with large active sites.

Recently, amorphous MoS_2 has also drawn the scientists' attention as efficient catalysts for HER because it contains many active unsaturated sulfur atoms.[10] However, the poor crystallinity of the amorphous sulfide leads to relatively high solubility and poor electrochemical stability in the acid electrolyte, which limits their practical implications. Therefore, the development of MoS_2 nanocatalysts owning both abundant active edge sites and good crystallinity is an effective approach to simultaneously achieve high HER activity and long-term stability. Despite great progresses, controllable synthesis of ultrasmall MoS_2 with abundant active edge sites and good crystallinity towards high HER activity and high stability still remains as a great challenge. Herein, we report a facile strategy to synthesize the highly active and stable ultrasmall donut shaped Cu_7S_4@MoS_2 hetero-nanoframes with abundant active MoS_2 edge sites for HER. These nanoframes achieved a current density of 200 mA cm^{-2} at an overpotential of 206 mV, a Tafel slope of 48 mV/decade, and excellent stability over 5000 cycles in 0.5 M of H_2SO_4 media.

The Cu_7S_4@MoS_2 nanoframes were prepared by hot-injection where the lab-made Mo-based precursors were injected to the as-prepared Cu_7S_4 nanoparticles (NPs)[11] colloidal solution while maintaining the temperature at 300 °C for 10 min (see Supporting Information for details). Transmission electron microscope (TEM) images revealed that a heterostructure nanoframe (Figure 1 a) with uniform shape and size was formed after the addition of Mo-based precursors to the as-prepared Cu_7S_4 colloids (Figure 1 b) where the main body of Cu_7S_4 has been etched. The high-resolution transmission electron microscope (HRTEM)

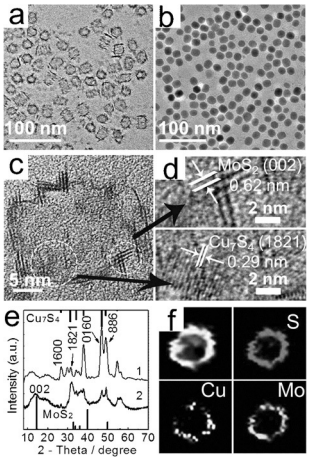

Figure 1. TEM (a,b), HRTEM (c,d) images, XRD patterns (e) and elemental mapping (f) of Cu_7S_4@MoS_2 nanoframes (a,c–f) obtained after treatment at 300 °C for 10 min, and of Cu_7S_4 (b,e).

[*] J. Xu,[+] J. B. Cui,[+] C. Guo, R. Jiang, Prof. S. Y. Xu, Z. B. Zhuang, Prof. Dr. L. Y. Wang
State Key Laboratory of Chemical Resource Engineering
Beijing University of Chemical Technology
Beijing 100029 (China)
E-mail: lywang@mail.buct.edu.cn
Z. P. Zhao, Prof. Dr. Y. Huang
Department of Materials Science & Engineering
University of California Los Angeles, CA 90095 (USA)
Prof. Dr. Y. D. Li
Department of Chemistry, Tsinghua University
Beijing, 100086 (China)
[+] These authors contributed equally to this work.

Supporting information for this article can be found under: http://dx.doi.org/10.1002/anie.201600686.

image (Figure 1 c,d) and X-ray diffraction (XRD) patterns (Figure 1 e) evidenced the presence of Cu_7S_4 (JCPDS No. 23-0958) and MoS_2 (JCPDS No. 73-1508) in the nanoframe. Compared to the XRD pattern of Cu_7S_4, the strong diffraction peaks of Cu_7S_4 dramatically weakened in the pattern of nanoframes, suggesting the etching of Cu_7S_4 and growing of MoS_2. The formation of MoS_2 was also confirmed through the appearance of typical absorption around 650 nm of MoS_2 nanocrystals[12] and the disappearance of the localized surface plasmon resonance (LSPR) peak around 1500 nm of Cu_7S_4 nanoparticles[11] (Figure S1 in the Supporting Information). It is noteworthy that sulfur is necessary in the Mo-based precursor solution for the fabrication of Cu_7S_4@MoS_2 nanoframes. Without it we do not obtain the nanoframe structure (Figure S2). In addition, HRTEM images also indicated that the newly formed MoS_2 nanosheets, a few layers thick (1–3 layers), with an average length of 5.2 ± 1.3 nm were distributed at the edge of Cu_7S_4. Meanwhile, the width of the MoS_2 nanosheets is very narrow, just a few of nanometers. The resolved lattice fringes of MoS_2 (002) planes with an interplanar spacing of 0.62 nm and Cu_7S_4 (1821) planes with an interplanar spacing of 0.29 nm were clearly revealed (Figure 1 d). The elemental mapping indicated a relatively homogenous distribution of each element along the nanoframe (Figure 1 f). The chemical states of Mo, Cu, and S elements in the Cu_7S_4@MoS_2 nanoframe were further confirmed via X-ray photoelectron spectroscopy (XPS) analysis (Figure S3). To enhance the catalytic activity, many nanocatalysts have been fabricated into nanoframes to greatly expose the active crystal facets, but they were mainly alloys or noble-metal nanostructures.[1d,13] The donut shape of our nanoframes with increased exposure of edge sites is believed to be beneficial for the catalytic performance in the HER.

The catalytic performance of these nanoframes was evaluated in terms of the abilities for H_2 production and the stability. The HER stability tests were carried out in H_2-saturated 0.5 M H_2SO_4 by performing linear scan with applied voltage potential ranging from 0.36 V to −0.44 V versus reversible hydrogen electrode (RHE), and all data were reported with iR compensation. All the catalyst-modified working electrodes were activated by cyclic voltammetry (CV) scanning for 11 000 cycles with carbon counter electrode before the electrocatalytic tests. The saturated calomel electrode (SCE) was used as the reference electrode and calibrated with respect to RHE (Experimental section, Figure S4). In addition, commercial Pt benchmark (20 % Pt/C) was also used as control experiments. As expected, Pt/C shows superior HER activity with negligible overpotential (Figure 2 a). The nanoframes show an overpotential as low as 133 mV at 10 mA cm^{-2} with a Tafel slope of 48 mV dec^{-1} (Figure 2 b) and further increasing overpotential would cause a rapid rise of cathodic current (200 mA cm^{-2} with overpotential of 206 mV), suggesting the nanoframes have high performance for HER. As shown in Figure S5, if the nanoframe loaded working electrode was activated by CV scanning for 11 000 cycles with Pt wire counter electrode, at the current density of 10 mA cm^{-2}, the overpotential was decreased from 133 to 26 mV, demonstrating a better catalytic activity than that of commercial 20 % wt Pt/C. During the

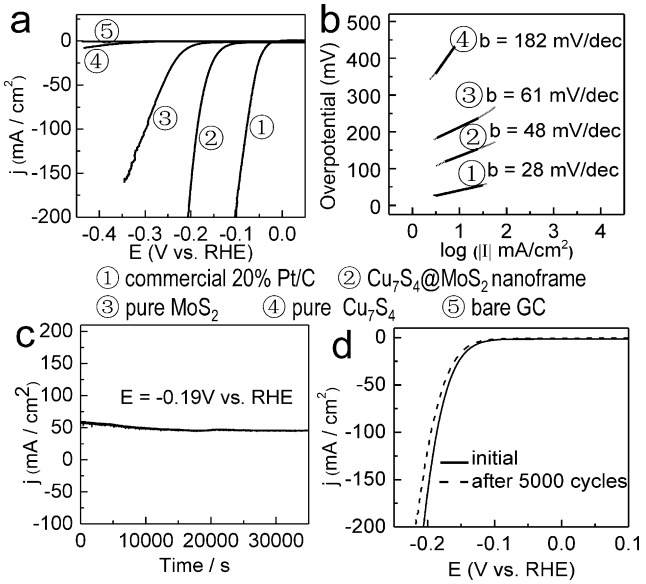

Figure 2. a) Polarization curves obtained on bare glass carbon (GC) electrode and modified GC electrodes with 20 % commercial Pt/C, Cu_7S_4@MoS_2 nanoframes, pure MoS_2 nanosheet, and pure Cu_7S_4 NPs. Catalyst loading is about 0.28 mg cm^{-2} for all samples. Sweep rate: 10 mV s^{-1}. b) Corresponding Tafel plots. c) Chronoamperometric responses (*j*–*t*) tested on as-prepared Cu_7S_4@MoS_2 nanoframes at a constant applied potential of −0.19 V versus RHE. d) Durability test for the nanoframes with 5000 cycles from +0.36 to −0.44 V versus RHE at 100 mV s^{-1}.

activation, the potential of Pt wire counter electrode was monitored and increased with the increase of current density (Table S1). The value of potential reached 2.214 V (vs. reversible hydrogen electrode (RHE)) when the current density was 200 mA cm^{-2}, which was far higher than the standard potential (1.18 V, vs. RHE) of Pt^{II}/Pt. Therefore, the Pt possibly dissolved from the Pt counter electrode and then deposited on the working electrode under the activation conditions, which has been confirmed through the Pt concentration in the electrolyte during the activation (Table S1). Therefore, this good catalytic activity can be attributed to the synergistic effects of abundant MoS_2 active edge sites and deposited Pt released from the Pt wire counter electrode. The deposited Pt on the working electrode was also carefully checked via inductively coupled plasma mass spectrometry (ICP-MS), and the concentration of Pt in the total catalysts (nanoframes + Pt) was 12.1 %, which is lower than that (20 %) in commercial Pt/C catalysts. These results suggest a potential way to get better activity with less Pt.

As a control, the pure Cu_7S_4 NPs and MoS_2 nanosheets prepared without the Cu_7S_4 templates (Experimental Section, Figure S6) were also checked and showed a poor HER activity. These results indicated that the formation of nanoframe heterostructure is crucial for the enhanced HER catalytic efficacy. Compared to the reported MoS_2 and other non-Pt HER catalysts using carbon electrode as the counter electrode (Table S2), our nanoframes demonstrate comparable or more efficient activity. To further demonstrate the importance of the frame structure for HER, we removed the Cu_7S_4 template by incubating the nanoframes with ammonia

(Figure S7). Compared to the nanoframes, the as-obtained MoS_2 demonstrated a far lower catalytic activity for HER (Figure S8), which can be attributed to the MoS_2 aggregation and thus the decrease of active edge sites. Meanwhile, if we increase the Mo-precursor dosage from 0.2 to 0.4 mmol using the same method for Cu_7S_4@MoS_2 nanoframes, only low-activity small nanodots instead of Cu_7S_4@MoS_2 nanoframes were obtained (Figure S9), further suggesting the Cu_7S_4 template supporting is crucial to maintain the full exposure of the active edge sites of MoS_2 for the good catalytic activity. We also checked the stability of these nanoframe catalysts under electrocatalytic conditions. As shown in Figure S10, after incubation with 0.5 M H_2SO_4 for 24 h, the donut structure of the nanoframes is well maintained, unlike that of nanoframes being treated with $NH_3{\cdot}H_2O$ (Figure S7b), suggesting that these nanoframes are stable under the electrocatalytic conditions.

As shown in Figure 2b, the Tafel slope for Pt/C is measured about 28 mV dec^{-1}, which is consistent with the reported value. The Cu_7S_4@MoS_2 nanoframe exhibits a small Tafel slope of 48 mV/dec in the low current density region, which is comparable to or even smaller than those of many Mo-based HER catalysts (Table S2). Additionally, the Tafel slope also reveals the HER catalyzed by our nanoframes proceeds through the Volmer–Heyrovsky mechanism.[14] By contrast, the pure Cu_7S_4 and MoS_2 show a larger Tafel slope of 182 and 61 mV dec^{-1}, respectively, again demonstrating the effectiveness of the nanoframe catalysts. The value of exchange current density of Cu_7S_4@MoS_2 nanoframes is calculated to be 1.9×10^{-2} mA cm^{-2} by extrapolating the Tafel plot (Figure S11), which is comparable to or even higher than that of most non-Pt HER catalysts.

The long-term stability and durability of our nanoframes acting as HER catalysts was examined using chronoamperometry (*j–t*) at a constant potential of −0.19 V versus RHE. As shown in Figure 2c, a stable current density of about 50 mA cm^{-2} was observed through the 35000 s continuous operation, implying its good durability under HER conditions. The electrochemical stability of the product was further proved by a long-term cyclic voltammetry cycling test at a scan rate of 0.1 V s^{-1} between −0.44 and +0.36 V versus RHE (Figure 2d). After 5000 cycles, there are negligible changes of the polarization curves, compared with that obtained prior to cycling test, which confirms the good stability of these nanoframe catalysts.

To investigate the effects of high-temperature treatment on the structure and further HER activity of these nanoframes, the colloidal solution was treated at 300 °C for 1, 3, 5, 10, and 20 min (Figure 3), after the injection of Mo-based precursors. The corresponding products were termed S_1, S_3, S_5, S_{10}, and S_{20}, respectively. Both TEM (Figure 3a–d, Figure S12) and HRTEM (Figure 3e–h) images present the evolution process of the nanostructure. At the first stage, the MoS_2 grew on the edge of Cu_7S_4 nanoparticle (Figure 3a,e). By prolonging the reaction time, more and more MoS_2 nanosheets were formed, and the main body of Cu_7S_4 was etched away. Finally, a donut shape of Cu_7S_4@MoS_2 nanoframes was obtained. By sweeping the potential from 0.36 to −0.44 V versus RHE at room temperature, with a sweep rate of 10 mV s^{-1}, the HER activity was evaluated for S_1–S_{20}. As shown in (Figure 3i), the HER activity was greatly enhanced with the prolonging of reaction time from 1 to 10 min, which can be attributed to the ever-increasing amount of MoS_2. Compared to S_{10} (Figure 1a), the S_{20} has no obvious difference in the shape, size, and HER activity, indicating that the Mo-based precursor has been used up after being treated at 300 °C for 10 min.

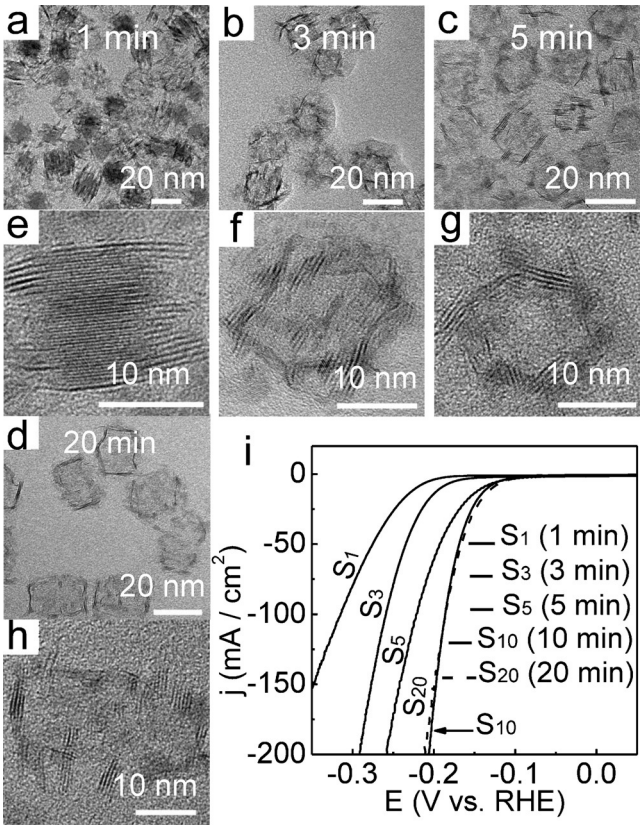

Figure 3. TEM (a–d) and HRTEM (e–h) images of Cu_7S_4@MoS_2 nanoframes prepared by heating treatment (300 °C) for 1 (a,e; S_1), 3 (b,f; S_3), 5 (c,g; S_5), and 20 min (d,h; S_{20}) after the addition of Mo-based precursors. i) Polarization curves obtained on glass carbon (GC) electrode modified with nanoframes.

In conclusion, we have presented a facile strategy for the synthesis of donut shape Cu_7S_4@MoS_2 nanoframes. These nanoframes are then uncovered as noble metal-free and non-precious catalysts and exhibit promising catalytic properties for HER with good stability. Specifically the nanoframes exhibit exceptionally high current density (200 mV cm^{-2} with 206 mV overpotential) for HER with Tafel slope of 48 mV dec^{-1}. We attributed the good performance to the abundant MoS_2 active edge sites. Since the solvothermal method is reasonably scalable, this study may open up a new route for the development of other non-expensive chalcogenide nanoframe catalysts with large quantities.

Experimental Section

Preparation of copper (Cu) precursors. In a typical reaction, 0.1 mmol of $Cu(NO_3)_2{\cdot}3H_2O$ and 0.05 mmol *N*,*N*′-dibutyldithiocarbamic acid HS_2CNBut_2 (DT) were dissolved in 1 mL of ethanol and stirred for

5 min to form a homogeneous solution. The prepared precursor, green $Cu(DT)_2$, was stored at room temperature for later use.

Preparation of molybdenum-based (Mo) precursors. 0.2 mmol $MoCl_5$ and 0.4 mmol sulfur (S) were, respectively dissolved in 1 mL of oleylamine and stirred for at least 30 min to form a homogeneous solution. Then the as-prepared S- and Mo-precursor solution were mixed and stirred for another 10 min, then stored at room temperature for later use.

Synthesis of ultrasmall Cu_7S_4@MoS_2 nanoframes. The Cu_7S_4 nanoparticles were synthesized according to our previously reported method with some modifications before the fabrication of Cu_7S_4@MoS_2 nanoframes.[11] In brief, 4.0 mL of oleylamine and 6.0 mL of 1-octadecene were mixed in a 50-mL three-necked flask. The solution was bubbled with nitrogen under vigorous magnetic stirring. Then the as-prepared $Cu(DT)_2$ precursor (0.1 mmol Cu^{2+}, 0.05 mmol DT) was added to the solution at 205 °C and then the temperature was kept at 190 °C for 15 min under nitrogen atmosphere with magnetic stirring. Thereafter, the temperature of the solution was rapidly raised to 310 °C. The as-prepared Mo-based precursor solution (0.2 mmol Mo^{5+}, 0.4 mmol S) was then injected into solution. After keeping the temperature at 300 °C for 10 min (It is of noted that the reaction time varied when investigating the morphology of hetero-nanostructures at different reaction times), the resulting solution was allowed to cool to room temperature. The product was collected by centrifugation and washed with cyclohexane. Other detailed experiments are shown in Supporting Information.

Acknowledgements

This research was supported in part by the National Natural Science Foundation of China (Grant Nos. 21475007 and 21275015).

Keywords: electrocatalysis · hydrogen-evolution reaction · molybdenum disulfides · nanoframes

How to cite: *Angew. Chem. Int. Ed.* **2016**, *55*, 6502–6505
Angew. Chem. **2016**, *128*, 6612–6615

[1] a) D. S. Kong, H. T. Wang, Z. Y. Lu, Y. Cui, *J. Am. Chem. Soc.* **2014**, *136*, 4897–4900; b) M. S. Faber, R. Dziedzic, M. A. Lukowski, N. S. Kaiser, Q. Ding, S. Jin, *J. Am. Chem. Soc.* **2014**, *136*, 10053–10061; c) D. Y. Wang, M. Gong, H. L. Chou, C. J. Pan, H. A. Chen, Y. P. Wu, M. C. Lin, M. Y. Guan, J. Yang, C. W. Chen, Y. L. Wang, B. J. Hwang, C. C. Chen, H. J. Dai, *J. Am. Chem. Soc.* **2015**, *137*, 1587–1592; d) L. Cheng, W. J. Huang, Q. F. Gong, C. H. Liu, Z. Liu, Y. G. Li, H. J. Dai, *Angew. Chem. Int. Ed.* **2014**, *53*, 7860–7863; *Angew. Chem.* **2014**, *126*, 7994–7997; e) J. Deng, P. J. Ren, D. H. Deng, X. H. Bao, *Angew. Chem. Int. Ed.* **2015**, *54*, 2100–2104; *Angew. Chem.* **2015**, *127*, 2128–2132; f) P. Jiang, Q. Liu, Y. H. Liang, J. Q. Tian, A. M. Asiri, X. P. Sun, *Angew. Chem. Int. Ed.* **2014**, *53*, 12855–12859; *Angew. Chem.* **2014**, *126*, 13069–13073; g) E. J. Popczun, C. G. Read, C. W. Roske, N. S. Lewis, R. E. Schaak, *Angew. Chem. Int. Ed.* **2014**, *53*, 5427–5430; *Angew. Chem.* **2014**, *126*, 5531–5534; h) J. Yang, D. Voiry, S. J. Ahn, D. Kang, A. Y. Kim, M. Chhowalla, H. S. Shin, *Angew. Chem. Int. Ed.* **2013**, *52*, 13751–13754; *Angew. Chem.* **2013**, *125*, 13996–13999.

[2] a) Y. Zheng, Y. Jiao, Y. H. Zhu, L. H. Li, Y. Han, Y. Chen, A. J. Du, M. Jaroniec, S. Z. Qiao, *Nat. Commun.* **2014**, *5*, 3873–3880; b) W. C. Sheng, Z. B. Zhuang, M. R. Gao, J. Zheng, J. G. G. Chen, Y. S. Yan, *Nat. Commun.* **2015**, *6*, 5848–5853; c) X. Huang, Z. Y. Zeng, S. Y. Bao, M. F. Wang, X. Y. Qi, Z. X. Fan, H. Zhang, *Nat. Commun.* **2013**, *4*, 1444–1451.

[3] a) V. S. Thoi, Y. J. Sun, J. R. Long, C. J. Chang, *Chem. Soc. Rev.* **2013**, *42*, 2388–2400; b) Y. F. Sun, S. Gao, F. C. Lei, Y. Xie, *Chem. Soc. Rev.* **2015**, *44*, 623–636; c) M. R. Gao, J. X. Liang, Y. R. Zheng, Y. F. Xu, J. Jiang, Q. Gao, J. Li, S. H. Yu, *Nat. Commun.* **2015**, *6*, 5982–5988; d) J. F. Xie, H. Zhang, S. Li, R. X. Wang, X. Sun, M. Zhou, J. F. Zhou, X. W. Lou, Y. Xie, *Adv. Mater.* **2013**, *25*, 5807–5813; e) J. F. Xie, J. J. Zhang, S. Li, F. Grote, X. D. Zhang, H. Zhang, R. X. Wang, Y. Lei, B. C. Pan, Y. Xie, *J. Am. Chem. Soc.* **2013**, *135*, 17881–17888.

[4] a) T. F. Jaramillo, K. P. Jorgensen, J. Bonde, J. H. Nielsen, S. Horch, I. Chorkendorff, *Science* **2007**, *317*, 100–102; b) H. I. Karunadasa, E. Montalvo, Y. Sun, M. Majda, J. R. Long, C. J. Chang, *Science* **2012**, *335*, 698–702.

[5] a) B. Hinnemann, P. G. Moses, J. Bonde, K. P. Jorgensen, J. H. Nielsen, S. Horch, I. Chorkendorff, J. K. Norskov, *J. Am. Chem. Soc.* **2005**, *127*, 5308–5309; b) C. Tsai, F. Abild-Pedersen, J. K. Norskov, *Nano Lett.* **2014**, *14*, 1381–1387.

[6] a) S. Shima, O. Pilak, S. Vogt, M. Schick, M. S. Stagni, W. Meyer-Klaucke, E. Warkentin, R. K. Thauer, U. Ermler, *Science* **2008**, *321*, 572–575; b) M. Asadi, B. Kumar, A. Behranginia, B. A. Rosen, A. Baskin, N. Repnin, D. Pisasale, P. Phillips, W. Zhu, R. Haasch, R. F. Klie, P. Kral, J. Abiade, A. Salehi-Khojin, *Nat. Commun.* **2014**, *5*, 4470–4477; c) Y. Zheng, Y. Jiao, M. Jaroniec, S. Z. Qiao, *Angew. Chem. Int. Ed.* **2015**, *54*, 52–65; *Angew. Chem.* **2015**, *127*, 52–66.

[7] a) M. A. Lukowski, A. S. Daniel, F. Meng, A. Forticaux, L. Li, S. Jin, *J. Am. Chem. Soc.* **2013**, *135*, 10274–10277; b) S. Huang, M. Bai, L. Y. Wang, *Sci. Rep.* **2013**, *3*, 2023–2027; c) D. Voiry, M. Salehi, R. Silva, T. Fujita, M. W. Chen, T. Asefa, V. B. Shenoy, G. Eda, M. Chhowalla, *Nano Lett.* **2013**, *13*, 6222–6227.

[8] a) X. Geng, W. Wu, N. Li, W. Sun, J. Armstrong, A. Al-hilo, M. Brozak, J. Cui, T.-p. Chen, *Adv. Funct. Mater.* **2014**, *24*, 6123–6129; b) H. T. Wang, Z. Y. Lu, D. S. Kong, J. Sun, T. M. Hymel, Y. Cui, *ACS Nano* **2014**, *8*, 4940–4947; c) L. Liao, J. Zhu, X. J. Bian, L. N. Zhu, M. D. Scanlon, H. H. Girault, B. H. Liu, *Adv. Funct. Mater.* **2013**, *23*, 5326–5333; d) J. P. Shi, D. L. Ma, G. F. Han, Y. Zhang, Q. Q. Ji, T. Gao, J. Y. Sun, X. J. Song, C. Li, Y. S. Zhang, X. Y. Lang, Y. F. Zhang, Z. F. Liu, *ACS Nano* **2014**, *8*, 10196–10204; e) Y. H. Chang, C. T. Lin, T. Y. Chen, C. L. Hsu, Y. H. Lee, W. J. Zhang, K. H. Wei, L. J. Li, *Adv. Mater.* **2013**, *25*, 756–760.

[9] a) J. Kibsgaard, Z. Chen, B. N. Reinecke, T. F. Jaramillo, *Nat. Mater.* **2012**, *11*, 963–969; b) B. Seo, G. Y. Jung, Y. J. Sa, H. Y. Jeong, J. Y. Cheon, J. H. Lee, H. Y. Kim, J. C. Kim, H. S. Shin, S. K. Kwak, S. H. Joo, *ACS Nano* **2015**, *9*, 3728–3739.

[10] a) D. Merki, S. Fierro, H. Vrubel, X. L. Hu, *Chem. Sci.* **2011**, *2*, 1262–1267; b) J. D. Benck, Z. B. Chen, L. Y. Kuritzky, A. J. Forman, T. F. Jaramillo, *ACS Catal.* **2012**, *2*, 1916–1923.

[11] a) J. B. Cui, R. Jiang, S. Y. Xu, G. F. H, L. Y. Wang, *Small* **2015**, *11*, 4183–4190; b) J. B. Cui, Y. J. Li, L. Liu, L. Chen, J. Xu, J. W. Ma, G. Fang, E. B. Zhu, H. Wu, L. X. Zhao, L. Y. Wang, Y. Huang, *Nano Lett.* **2015**, *15*, 6295–6301; c) J. B. Cui, S. Y. Xu, C. Guo, R. Jiang, T. D. James, L. Y. Wang, *Anal. Chem.* **2015**, *87*, 11592–11598.

[12] S. Xu, D. Li, P. Wu, *Adv. Funct. Mater.* **2015**, *25*, 1127–1136.

[13] Y. E. Wu, D. S. Wang, G. Zhou, R. Yu, C. Chen, Y. D. Li, *J. Am. Chem. Soc.* **2014**, *136*, 11594–11597.

[14] B. E. Conway, B. V. Tilak, *Electrochim. Acta* **2002**, *47*, 3571–3594.

Received: January 21, 2016
Revised: March 19, 2016
Published online: April 20, 2016

